

Contents lists available at ScienceDirect

Mechanical Systems and Signal Processing

journal homepage: www.elsevier.com/locate/ymssp



Robust fault detection in bond graph framework using interval analysis and Fourier-Motzkin elimination technique



Mayank Shekhar Jha a,*, Nizar Chatti b, Philippe Declerck b

- ^a Institut Clement Ader, INSA Toulouse, 3 rue Caroline Aigle, 31400 Toulouse Cedex, France
- ^b ISTIA, LARIS, EA, 7315, Angers University, 62 Avenue Notre Dame du Lac, 49000 Angers, France

ARTICLE INFO

Article history:
Received 28 April 2016
Received in revised form 10 January 2017
Accepted 12 February 2017

Keywords:
Interval analysis
Robust diagnosis
Uncertain systems
Bond graph modelling
Analytical Redundancy Relations

ABSTRACT

This paper addresses the fault diagnosis problem of uncertain systems in the context of Bond Graph modelling technique. The main objective is to enhance the fault detection step based on Interval valued Analytical Redundancy Relations (named I-ARR) in order to overcome the problems related to false alarms, missed alarms and robustness issues. These I-ARRs are a set of fault indicators that generate the interval bounds called thresholds, A fault is detected once the nominal residuals (point valued part of I-ARRs) exceed the thresholds. However, the existing fault detection method is limited to parametric faults and it presents various limitations with regards to estimation of measurement signal derivatives, to which I-ARRs are sensitive. The novelties and scientific interest of the proposed methodology are: (1) to improve the accuracy of the measurements derivatives estimation by using a dedicated sliding mode differentiator proposed in this work, (2) to suitably integrate the Fourier-Motzkin Elimination (FME) technique within the I-ARRs based diagnosis so that measurements faults can be detected successfully. The latter provides interval bounds over the derivatives which are included in the thresholds. The proposed methodology is studied under various scenarios (parametric and measurement faults) via simulations over a mechatronic torsion bar system.

© 2017 Elsevier Ltd. All rights reserved.

1. Introduction

An autonomous system is expected to achieve different objectives at given times without the intervention of a human operator. The increase in system complexity and industrial safety requirements has led to a growing interest for the development of fault diagnosis procedures. Fault diagnosis is crucial for ensuring the safe operation and prevention of unacceptable system behavior. The overall aim of a diagnosis procedure consists of fault detection (FD) and isolation as quickly as possible. Most of the fault detection and isolation (FDI) approaches rely mainly upon set of fault indicators. These indicators are so-called residuals which are generated such that the discrepancies between the expected system behavior and real behavior are captured efficiently. This issue has been addressed by using parity space technique [1,2], observer based techniques [3–5], data based techniques [6], parameters identification [7], graphical approaches [8], and so on. A comprehensive classification of these approaches can be found in [9–11]. Among the graphical approaches, the Bond Graph (BG) [12] as a multidisciplinary and unified graphical modelling language has proved its adequacy and efficiency to represent energy exchanges in multi- energetic systems. BG has been used extensively to generate fault indicators in a systematic and generic

E-mail addresses: Jha.mayank.jha@gmail.com (M.S. Jha), nizar.chatti@univ-angers.fr (N. Chatti).

^{*} Corresponding author.

Nomenclature

Abbreviations & Acronyms FD fault detection

FDI fault detection and isolation ARRs Analytical Redundancy Relations

BG Bond Graph

VAF Percentage Variance Accounted For

I-ARR Interval Valued Analytical Redundancy Relations

FME Fourier-Motzkin Elimination

presents a strong motivation.

URIF Uncertain Residual Interval Function (URIF)

AME Absolute Mean Error IoA Index of Agreement

way. The BG model can be exploited, due to its structural and causal properties, for automatic generation of Analytical Redundancy Relations (ARRs), numerical evaluation of which produce residuals that are used for diagnosis. These ARRs are mathematical constraints used to verify the coherence between the process measurements and system model. ARR generation technique that exists within the realm of BG modelling [13] has been extensively exploited in last one decade. The latter includes *covering causal paths* technique which has successfully been used for supervision of highly non-linear and complex thermo-chemical systems [14,15], non-linear mechatronic systems [16,17], intelligent and autonomous systems [18], industrial chemical reactors [19], hybrid systems [20–24], etc.

The model uncertainties mainly arise due to discrepancy between the model and the real system such as measurement noise and variable environmental conditions. Uncertainties can be considered with respect to system parameters, system measurements or both, depending upon the modelling/user requirements. In this context, Bond Graph (BG) based works have been exploited extensively for efficient and robust passive diagnosis [25–28]. Very recently, modelling of system parameters and measurements in interval form has been proposed in [29], where model uncertainties (parametric and measurement uncertainties) are modelled as interval models. Then, interval valued uncertainties are used to generate Interval Valued Analytical Redundancy Relations (I-ARRs) which are evaluated using Interval Analysis (IA) [30–32]. A passive fault detection methodology is developed by exploiting the structural, causal aspects of BG and IA based calculations. Moreover, [33] proposes the I-ARR based methodology as FD module for robust detection of parametric degradation beginning. Therein, uncertainty is considered with respect to system parameters only; system measurements (sensors) are not considered uncertain. Although, the integration of IA with BG has resulted in successful alleviation of issues related to FD, residual evaluation and presence of parametric as well as measurement uncertainties, lead to significant issues that remain unaddressed.

- a. ARRs and I-ARRs are inevitably sensitive to derivative of system measurements. Differentiation of noisy measurement signals leads to significant noise in residuals. The latter leads to false alarms, hidden alarms, fault masking and robustness issues. Thus, minimization of noise over residuals has been a major research endeavor in the last decade. In present context, optimal estimation of measurement signal derivatives sensitive to I-ARRs is sought. To that end, a dedicated sliding mode differentiator is proposed in this paper which is shown to ameliorate the accuracy of measurement(s)-derivative(s). The proposed differentiator produces interval bounds over signal-differentiation. The latter, in turn, are included in the threshold generation process.
- b. Uncertain measurement intervals are generally non-linearly sensitive to system parameters in an I-ARR; this may not result in perfectly separable nominal and uncertain parts. Moreover, due to presence of measurement uncertainties, an I-ARR expression may remain sensitive to multiple interval variables. This leads to multiple incidence problem [36], thin interval enclosures [31] for Interval function range. The latter in turn results in over-estimation of thresholds [37], wrapping effects [38], etc. One of the efficient ways to overcome these problems, as proposed in this work, is to decouple the FD reasoning strategy for uncertain system measurements from that of uncertain system parameters. To that end, Fourier-Motzkin Elimination (FME) technique which is a computational method for solving linear inequalities by iterative elimination of variables [34], is exploited. FME was introduced by Fourier in 1827; it was rediscovered in Motzkin's thesis in 1936. This finite algorithm enables to find a solution of a linear inequality system $A \cdot x \leq B$. Recently, various works have exploited FME for resolving optimization problems in operational research field. FME has also been extensively used to solve system of linear inequalities for real and integer solution spaces and solution of node-capacitated routing problem in an undirected ring network (for simple matrices) [35]. In the context of I-ARR enabled FD, I-ARRs are usually expressed as linear combination of functions of system parameters and measurements. As a result, the residuals bounded within upper and lower limits, may be treated as system of linear inequalities. Benefits of FME can be exploited for FD reasoning. It is worth noting that FME theory has never been applied in FD context. Thus, integration of the benefits of Interval Analysis and FME in Bond graph framework

Thus, in summary, the scientific interest of the paper is to ameliorate I-ARR enabled FD methodology in two major steps: (1) enhancement of signal measurement(s)-differentiation(s) accuracy by using a dedicated sliding mode differentiator, (2) suitable integration of Fourier-Motzkin Elimination (FME) technique within the I-ARRs enabled FD methodology for efficient FD. Moreover, this work also serves as the continuation of [33] with measurement uncertainties being taken into account.

The proposed methodology is studied under various scenarios (parametric and measurement faults) via simulations over a mechatronic torsion bar system. Apart from the Introduction section, the paper has 4 more sections. In Section 2, Uncertain BG, I-ARRs, FME techniques are introduced and discussed. Moreover, the existing issues are presented through illustrative examples. Additionally, a sliding mode differentiator is presented and a comparative study is made to assess the betterment in performance. In Section 3, the fault detection methodology is detailed and discussed. In Section 4, the mechatronic system is exploited for simulations, fault injection and fault detection. Section 5 draws conclusions.

2. Background and problem formulation

Firstly, the pre-requisite techniques are discussed in brief.

2.1. Uncertain BG and I-ARR derivation

The basics of BG modelling, interval valued representation of uncertainty and I-ARR derivation technique are omitted in this paper. The latter can be referred in [33] where a concise introduction is available with extensive literature references. In this section, authors have made an attempt to illustrate *I-ARR* generation method using a pedagogical example.

Example 1. Consider a pedagogical R-L-C electrical circuit as shown in Fig. 1a. The circuit current i through resistor R_1 , inductor L_1 and capacitor C_1 is i_m and the measured voltage across the capacitor is V_m .

Deterministic Diagnosis: Diagnosis oriented BGs are constructed in preferred derivative causality [39]. Moreover, the sensors are dualized implying that effort (flow) sensors De(Df) become sources of effort SSe (flow SSf) [40]. Following the aforementioned techniques, the diagnosis oriented BG of the nominal system is obtained in Fig. 1b. It should be noted that BG (see Fig. 1b) is constructed in derivative causality with dualized sensors ($SSf:i_m$ and $SSe:V_m$).

Analytical Redundancy Relations (ARRs) are obtained from the over-constrained (redundant and observable) subsystems that compose the overall system. ARRs are formulated using only known variables of the system [26,28,41]. They have the form f(k) = 0 for any function f. Numerical evaluation of an ARR yields a residual f = Eval[f(K)]. From Fig. 1b, two independent ARRs can be derived by elimination of unknown variables according to covering-causal paths (reaching the unknown variables by known ones through cause-effect relationships) as,

$$ARR_1:\ U(t)-L_1\frac{d\{SSf:i_m\}}{dt}-R_1\{SSf:i_m\}-\{SSe:V_m\}=0 \eqno(1)$$

$$ARR_2: \{SSf: i_m\} - C_1 \frac{d\{SSe: V_m\}}{dt} = 0$$
 (2)

Under fault free conditions, the residuals (numerical evaluation of ARRs) are theoretically equal to zero.

Robust Diagnosis with Interval valued Uncertainties: To highlight the existing issues, first, only system parameters are considered uncertain. In the subsequent part, uncertain parameters and uncertain system measurements are considered together for diagnosis [29]. Uncertain system parameters are considered as intervals where the upper and lower bounds are formed by taking parametric variation into account. In fact, for a system parameter θ with its nominal value as θ_n , $\Delta\theta_l \geq 0$ and $\Delta\theta_u \geq 0$ are the additive uncertainty/deviation on the left and right sides respectively over the nominal value θ_n ; $[\theta_n, \theta_n]$ is a degenerate interval (interval with equal upper and lower limits). Multiplicative interval uncertainty $[\delta_{\theta J}, \delta_{\theta J}]$

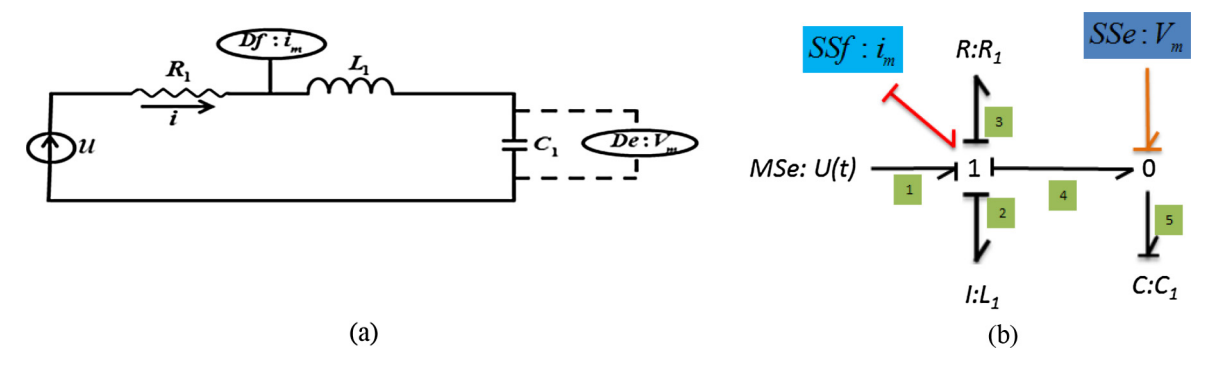


Fig. 1. Pedagogical example, (a) pedagogical RLC circuit and (b) BG model of the nominal system in derivative causality and dualized sensors.

is expressed as $\left[\delta_{\theta,l},\delta_{\theta,u}\right] = \left[\frac{-\Delta\theta_l}{\theta_n},\frac{-\Delta\theta_u}{\theta_n}\right]$. In this way, the uncertain parameter θ is also expressed as $\left[\theta_l,\theta_u\right] = \theta_n \cdot \left(1 + \left[\delta_{\theta,l},\delta_{\theta,u}\right]\right)$. In the context of Example 1, consider R_1 , C_1 and L_1 as uncertain system parameters. These parameters are modelled in interval form: $\left[R_{1,l},R_{1,u}\right] = R_{1,n}\left(1 + \left[\delta_{R_1,l},\delta_{R_1,u}\right]\right)$, $\left[C_{1,l},C_{1,u}\right] = C_{1,n}\left(1 + \left[\delta_{C_1,l},\delta_{C_1,u}\right]\right)$ and $\left[L_{1,l},L_{1,u}\right] = L_{1,n}\left(1 + \left[\delta_{L_1,l},\delta_{L_1,u}\right]\right)$. The uncertain BG is shown in Fig. 2, wherein the additional effort(s)/flow(s) (bonds 7, 8 and 10) being generated by interval valued uncertainty is(are) brought-in at BG junctions by fictitious sources of effort(s)/flow(s) ($MSe:[w_{R_1}],MSe:[w_{L_1}]$ and $MSe:[w_{C_1}]$). For instance, under nominal conditions, the constitutive relation for resistor element R is $e_i = R \times f_i$, where e_i is the effort and f_i is the flow variable on ith bond. Then, with interval-valued R_1 ,

$$[e_{6,l}, e_{6,u}] = [R_{1,l}, R_{1,u}] \cdot f_6 = R_{1,n} \left(1 + \left[\delta_{R1,l}, \delta_{R1,u} \right] \right) \cdot f_6 = \underbrace{R_{1,n} f_6}_{e_3} - \underbrace{\left(-\left[\delta_{R1,l}, \delta_{R1,u} \right] \cdot R_{1,n} \cdot f_6 \right)}_{e_7}$$
(3)

where $MSe: [w_{R1}]$ denotes the fictitious source of uncertain effort e_7 (see (3) and Fig. 2). Similarly, various other parametric uncertainties are taken into account in order to construct Fig. 2.

Recently, measurement uncertainties have also been taken into account over BG models [29]. An uncertain flow detector (carrying measured flow signal) is modelled as:

$$\left[\underline{SSf}, \overline{SSf}\right]_{measure} = \left[\underline{SSf_t}, \overline{SSf_t}\right]_{true} + \left[-\Delta SSf_l, \Delta SSf_u\right].$$

The uncertainty interval $[-\Delta SSf_1, \Delta SSf_u]$ is modelled by virtual source of flow $MSf^*: [-\Delta SSf_1, \Delta SSf_u]$ (denoted as $MSf^*: [\zeta_{SSf}]$). In the context of Example 1, $SSf: i_m$ and $SSe: V_m$ are considered uncertain. They are modelled on BG (see Fig. 2), such that relations (4) and (5) are obeyed. The latter lead to development of BG shown in Fig. 3.

$$\left[\underline{i_m}, \overline{i_m}\right]_{true} = SSf : i_m - \underbrace{MSf^* : (-[-\Delta SSf_{i_m,l}, \Delta SSf_{i_m,u}])}_{MSf^* : [\zeta_{SSf,im}]}$$
(4)

$$\underline{\left[V_{m}, \overline{V_{m}}\right]_{true}} = SSf : V_{m} - \underbrace{MSf^{*} : \left(-\left[-\Delta SSf_{V_{m},l}, \Delta SSf_{V_{m},u}\right]\right)}_{MSf^{*} : \left[\zeta_{SSf,V_{m}}\right]} \tag{5}$$

In Fig. 3, one I-ARR can be derived from observable junction 1_1 [33] as:

$$[IARR_1(t), \overline{IARR_1(t)}] = Ir_{1,n}(t) + [B_1(t), \overline{B_1(t)}]$$
(6)

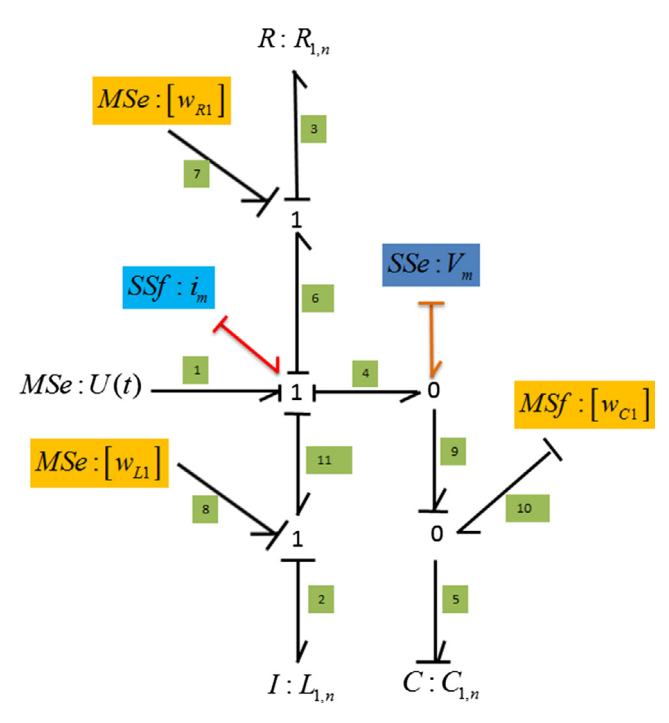


Fig. 2. BG of RLC circuit (Fig. 1) with interval valued uncertain system parameters R_1 , C_1 and L_1 .

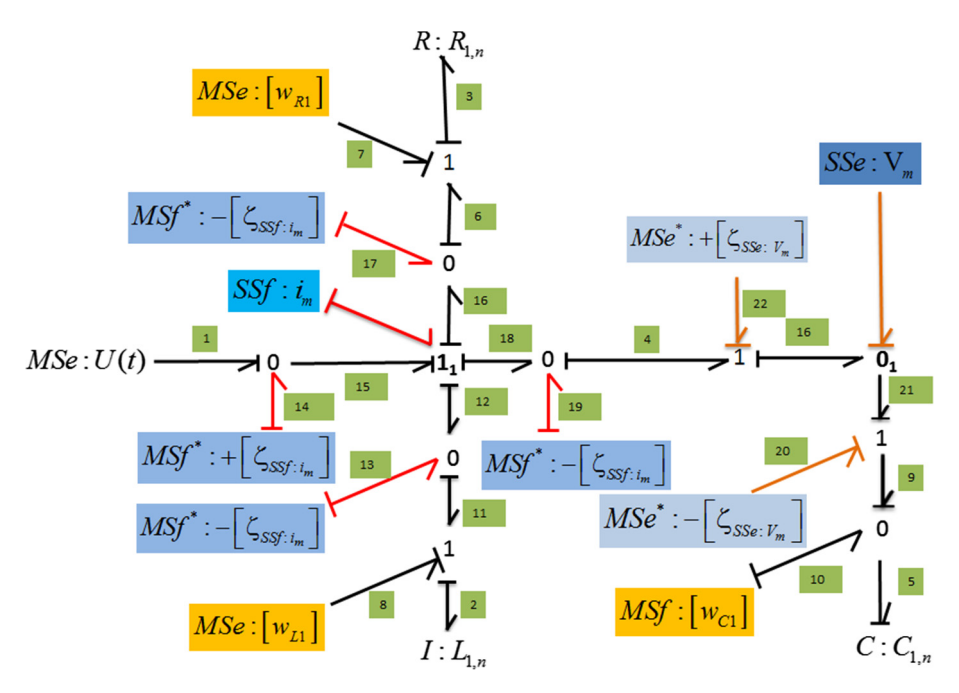


Fig. 3. BG of RLC circuit (Fig. 1) with interval valued uncertain system parameters R_1 , C_1 and L_1 and uncertain measurements i_m and V_m .

$$Ir_{1,n}(t) = U(t) - L_1 \frac{d\{SSf : i_m\}}{dt} - R_1\{SSf : i_m\} - \{SSe : V_m\}$$
 (7)

$$\underbrace{[\underline{B_1(t)},\overline{B_1(t)}]}_{\begin{subarray}{c} Parametric \\ Uncertainty \end{subarray}} \underbrace{-\left([\underline{L_1},\overline{L_1}]\cdot\frac{d([\zeta_{SSf:i_m}])}{dt}+([\underline{R_1},\overline{R_1}])(MSf:-[\zeta_{SSf:i_m}])+(MSe:-[\zeta_{SSe:V_m}])\right)}_{\begin{subarray}{c} Measurement \\ Uncertainty \end{subarray}}$$

where Ir is the nominal part of the I-ARR (sensitive to nominal value of parameters and point valued system variables) referred-to as *nominal residual* and $[\underline{B_1(t)}, \overline{B_1(t)}]$ is the interval valued part (sensitive to intervals) referred-to as *Uncertain Residual Interval Function* (URIF). Under faulty conditions, $(-Ir_{1,n}(t)) \notin [\underline{B_1(t)}, \overline{B_1(t)}]$ (see [29,33] for proof). Range of URIF is obtained by a set of finite sequence of steps, involving interval arithmetic as detailed in [29,33].

2.2. Major issues at hand

There are two major issues related with efficient evaluation of URIF range. These limitations arise due to the presence of measurement uncertainty intervals.

- 1. Multi-incident interval variables: Presence of multi-incident intervals in an interval function lead to over-estimation of range [37] and wrapping effects [38]. This classic problem leads to over-estimation of interval range and thin interval enclosures [31]. The I-ARR derived at an observable junction is sensitive to measurement uncertainty intervals. As such, a particular measurement uncertainty interval can manifest multiple times in an I-ARR, depending upon the number of BG elements to which the junction is sensitive. For instance, URIF of (8) is sensitive to multiple occurring ≤ [−ΔSSf_{im,l}, ΔSSf_{im,u}]. In complex systems, this problem may escalate significantly depending upon the number of BG elements that are sensitive to the BG junction at which a particular I-ARR is derived. Thus, there is a necessity to develop FD reasoning so that measurement uncertainties are not considered for URIF range evaluation (or threshold generation).
- 2. Estimation of signal derivative(s): The I-ARR expressions are mostly sensitive to derivatives (single or multiple order) of measurement signals. These derivatives manifest in the point valued *nominal residual* and URIF. As of present, the estimation of interval bounds over derivative of interval valued signals is done using finite difference of successive intervals. For instance, URIF of (8) is sensitive to $d(|\zeta_{SSF,im}|)/dt$ which is approximated as,

with.

$$\left[-\Delta SSe_{i_m,l},\Delta SSe_{i_m,u}\right]_{t_i} - \left[-\Delta SSe_{i_m,l},\Delta SSe_{i_m,u}\right]_{t_{i-1}} = \left[-\Delta SSe_{i_m,l,t_i} - \Delta SSe_{i_m,u,t_{i-1}},\Delta SSe_{i_m,u,t_i} + \Delta SSe_{i_m,l,t_{i-1}}\right] \tag{10}$$

where t_i is the discrete time index. Finite-difference method is a worst case approximation. As such, efficient methods are required for optimal approximation of the measurement derivative interval. The above mentioned issues are dealt respectively, by exploiting FME and sliding-mode differentiator as discussed below.

2.2.1. Fourier-Motzkin (FME) Elimination

To alleviate the aforementioned issues, FME is exploited for FD reasoning with respect to uncertain measurements. FME finds the solution(s) of a given linear system of inequalities: $A \cdot x \leq B$ where $A \in \mathbb{R}^{m,n}$ and $B \in \mathbb{R}^m$. Firstly, following notations are considered:

$$I^+ = \{i : a_{i1} > 0\}, \quad I^0 = \{i : a_{i1} = 0\}, \quad I^- = \{i : a_{i1} < 0\}, \quad a'_{ii} = a_{ii}/|a_{i1}|, \quad b'_i = b_i/|a_{i1}|$$

A system of inequalities $A \cdot x \leq B$ can be written in component form as:

$$\begin{cases}
a_{11} \cdot x_1 + a_{12} \cdot x_2 + \dots + a_{1n} \cdot x_n \leq b_1 \\
a_{21} \cdot x_1 + a_{22} \cdot x_2 + \dots + a_{2n} \cdot x_n \leq b_2 \\
\vdots \\
a_{n1} \cdot x_1 + a_{n2} \cdot x_2 + \dots + a_{mn} \cdot x_n \leq b_m
\end{cases}$$
(11)

The objective remains in elimination of x_1 from system (11) and deduction of upper–lower bounds over certain interval of x_1 using x_2, x_3, \dots, x_n . For each row i, where $a_{i1} \neq 0$, the i^{th} inequality $\sum_{j=1}^n a_{ij} \cdot x_j \leq b_i$ is multiplied by $\frac{1}{|a_{i1}|}$.

Hence, system (1) leads to an equivalent system as follows:

$$\begin{cases} x_{1} + a'_{i2} \cdot x_{2} + \dots + a'_{in} \cdot x_{n} \leqslant b'_{i} & \text{for } i \in I^{+} \\ a_{i2} \cdot x_{2} + \dots + a_{in} \cdot x_{n} \leqslant b_{i} & \text{for } i \in I^{0} \\ -x_{1} + a'_{i2} \cdot x_{2} + \dots + a'_{in} \leqslant b'_{i} & \text{for } i \in I^{-} \end{cases}$$
(12)

It follows that x_2, x_3, \dots, x_n are the solution of the original system (11) if and only if x_2, x_3, \dots, x_n satisfy [42]:

$$\begin{cases}
\sum_{j=2}^{n} a_{ij} \cdot x_{j} \leq b_{i} & \text{for } i \in I^{0} \\
\sum_{j=2}^{n} a'_{kj} \cdot x_{j} - b'_{k} \leq x_{1} \leq a'_{i} - \sum_{j=2}^{n} a'_{ij} \cdot x_{j} & \text{for } i \in I^{+} \text{ and } k \in I^{-}
\end{cases}$$
(13)

Hence, with respect to system (12), it can be deduced that x_1 satisfies:

$$\max_{(k \in I^{-})} \left(\sum_{j=2}^{n} a'_{kj} \cdot x_j - b'_k \right) \leqslant x_1 \leqslant \min_{(i \in I^{+})} \left(b'_i - \sum_{j=2}^{n} a'_{ij} \cdot x_j \right) \tag{14}$$

The same procedure is iterated in order to obtain existential condition for upper and lower bound of x_2, x_3, \dots, x_n .

The complexity of calculation for each iteration is of the order of $k^2/4$ where k is the number of constraints in the system of inequalities. An illustrative example is considered.

Example 2. Consider the two linear equations as shown in (15) with variables x_i , (i = 1, ..., 3) such that their upper and lower limits are known. The latter are considered in (16) and (17). Each of the variables are also bound by a set of constraints (18), (19) and (20).

$$r_1 = a_1 x_1 + b_1 x_2 + c_1 r_2 = a_2 x_2 + b_2 x_3 + c_2$$
 (15)

where a_1 , b_1 , c_1 , a_2 , b_2 , $c_2 > 0$.

Consider the upper and lower bounds on the linear system as,

$$q_1 \leqslant r_1 \leqslant q_2 \tag{16}$$

$$l_1 \leqslant r_2 \leqslant l_2 \tag{17}$$

$$i_1 \leqslant x_1 \leqslant i_2$$
 (18)

$$j_1 \leqslant x_2 \leqslant j_2 \tag{19}$$

$$k_1 \leqslant x_3 \leqslant k_2 \tag{20}$$

Step 1: Elimination of x_1 Using (15) and adding (16) and (17),

$$q_1 + l_1 \le a_1 x_1 + (b_1 + a_2) x_2 + b_2 x_3 + c_1 + c_2 \le q_2 + l_2$$
 (21)

Eqs. (18) and (21) imply,

$$\max\left(i_1, \frac{(q_1+l_1)-(b_1+a_2)x_2-b_2x_3-c_1-c_2}{(a_1)}\right)\leqslant x_1\leqslant \min\left(i_2, \frac{(q_2+l_2)-(b_1+a_2)x_2-b_2x_3-c_1-c_2}{(a_1)}\right) \tag{22}$$

Eq. (22) implies,

$$i_1 \le i_2$$
 $a_1 + l_1 \le a_2 + l_2$
(23)

$$i_1 \leqslant \left(\frac{(q_2 + l_2) - (b_1 + a_2)x_2 - b_2x_3 - c_1 - c_2}{(a_1)}\right) \tag{24}$$

$$\left(\frac{(q_1+l_1)-(b_1+a_2)x_2-b_2x_3-c_1-c_2}{(a_1)}\right)\leqslant i_2\tag{25}$$

Step 2: Elimination of x_2

While (23) is a redundant information, (24), (25) and (19) lead to,

$$\max\left(j_1, \frac{(q_1+l_1)-b_2x_3-c_1-c_2-a_1i_2}{(b_1+a_2)}\right)\leqslant x_2\leqslant \min\left(j_2, \frac{(q_2+l_2)-b_2x_3-c_1-c_2-a_1i_1}{(b_1+a_2)}\right) \tag{26}$$

Eq. (26) implies,

$$\begin{aligned}
 j_1 &\leq j_2 \\
 q_1 + l_1 &\leq q_2 + l_2
 \end{aligned}
 \tag{27}$$

$$j_1 \leqslant \left(\frac{(q_2 + l_2) - b_2 x_3 - c_1 - c_2 - a_1 i_1}{(b_1 + a_2)}\right) \tag{28}$$

$$\left(\frac{(q_1+l_1)-b_2x_3-c_1-c_2-a_1i_2}{(b_1+a_2)}\right)\leqslant j_2 \tag{29}$$

Step 3: Elimination of x_3

Similar to the previous step, (27) gives redundant information and (28), (29) and (20) lead to,

$$\max\left(k_1, \frac{(q_1+l_1)-j_2(b_1+a_2)-c_1-c_2-a_1i_2}{(b_2)}\right) \leqslant x_3 \leqslant \min\left(k_2, \frac{(q_2+l_2)-j_1(b_1+a_2)-c_1-c_2-a_1i_1}{(b_2)}\right) \tag{30}$$

For notational simplicity, (30) is represented as,

$$x_{3,FME} \leqslant x_3 \leqslant \overline{x_{3,FME}} \tag{31}$$

Eq. (30) leads to following conditions,

$$k_1 \leqslant \frac{(q_2+l_2)-j_1(b_1+a_2)-c_1-c_2-a_1i_1}{(b_2)} \\ \frac{(q_1+l_1)-j_2(b_1+a_2)-c_1-c_2-a_1i_2}{(b_2)} \leqslant k_2$$
 (32)

Eq. (32) is a necessary condition for the existence of a feasible set of solution(s) in terms of known constants (coefficients sensitive to linear inequalities (16) and (17)). Moreover, x_3 can be found bounded in (30) by known constants. However, unlike (30), (22) and (26) generate bounds in terms of unknown variables. The unknown variables must be eliminated to generate the limits in terms of known constants. To this end, backward propagation by substitution of known constants is executed as discussed below.

Step 5: Starting from (26), specific sequences of operations are executed in order to eliminate unknown variables as:

1. $[-(b_2)\times \text{Eq. } (30) + (b_1+a_2)\times \text{Eq. } (26)]/(b_1+a_2)$ gives:

$$\begin{aligned} & \max(j_1, \frac{(q_1 - q_2) + (l_1 - l_2) + a_1(i_1 - i_2) + j_1(b_1 + a_2)}{b_1 + a_2}) \leqslant x_2 \leqslant \min(j_2, \frac{(q_2 - q_1) + (l_2 - l_1) + a_1(i_2 - i_1) + j_2(b_1 + a_2)}{b_1 + a_2}) \\ & \equiv x_{2.\mathit{FME}} \leqslant x_2 \leqslant \overline{x_{2.\mathit{FME}}} \end{aligned}$$

2.
$$[-(b_2) \times \text{Eq. } (30) + (b_1 + a_2) \times \text{Eq. } (33) + (a_1) \times \text{Eq. } (22)]/(a_1) \text{ gives:}$$

$$\max \left(i_1, \frac{2(q_1 - q_2) + 2(l_1 - l_2) + 2a_1i_1 - a_1i_2 + (j_1 - j_2)(b_1 + a_2)}{a_1}\right) \leqslant x_1 \leqslant \min \left(i_2, \frac{2(q_2 - q_1) + 2(l_2 - l_1) + 2a_1i_2 - a_1i_1 + (j_2 - j_1)(b_1 + a_2)}{a_1}\right)$$

$$\equiv x_{1.FME} \leqslant x_1 \leqslant \overline{x_{1.FME}}$$
(34)

Thus, given that existential condition (32) is obeyed, upper and lower bounds on each of the variables can be found in terms of known constants given in (30), (33) and (34). Clearly, FME leads to optimal boundaries over the system variables. In the FD context, such variables x_i , (i = 1, ..., 3) are analogous to a dynamical-system measurements and constants a_1 , b_1 , c_1 , a_2 , b_2 , c_2 are analogous to dynamical system parameters.

2.2.2. Numerical differentiator

To enable optimal estimation of the bounds on derivatives of noisy signals that are inevitably involved in evaluation of residuals, a first-order sliding mode differentiator is proposed.

2.2.2.1. Sliding mode differentiator. Let y be a signal to be differentiated, z_0 be an estimate of the signal to be derived and z_1, \ldots, z_n be the estimated derivatives. Note that $y = y_0 + e$ where e is a bounded Lebesgue-measurable noise with unknown Lipschitz constant and y_0 is an unknown base signal with n^{th} derivative having a known Lipschitz constant L > 0, which satisfies:

$$\left| y_0^{(n)}(t) - y_0^{(n)}(t-1) \right| \leqslant L \cdot \Delta t$$
 (35)

The equations of the 1st order differentiator (given in Fig. 4) can be written as follows:

$$\begin{cases} \dot{z}_0 = -\alpha_0 \cdot \sqrt{|z_0 - y(t)|} \operatorname{sign}(z_0 - y(t)) + z_1 \\ \dot{z}_1 = -\alpha_1 \cdot \operatorname{sign}(z_0 - y(t)) \end{cases}$$
(36)

where z_1 and z_0 are the states of the differentiator, y is the signal to be differentiated. α_0 and α_1 are the parameters that must be tuned. The latter depend on the Lipschitz's constant L as [43],

$$\begin{array}{l} \alpha_0 = \sqrt{L} \\ \alpha_1 = 1 \cdot 1L \end{array} \tag{37}$$

The variable z_0 serves as an estimate for y while z_1 converges towards the required derivative \dot{y} . The advantage of using this sliding mode differentiator is that it also assesses the accuracy of estimated derivative of the measured signal. This accuracy denoted as ε_1 , can be calculated as follows [44]:

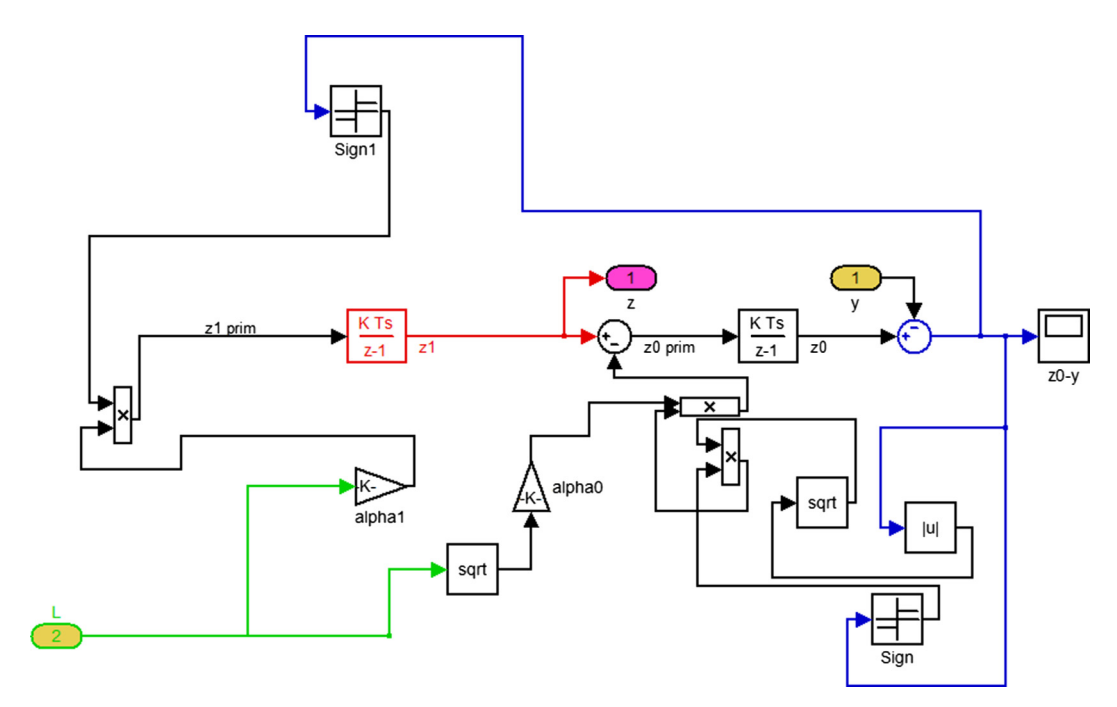


Fig. 4. Simulation block of the proposed sliding mode differentiator.

$$\varepsilon_1 = \mu_1 \cdot \sqrt{L} \cdot (\bar{e})^{\left(-\frac{1}{2}\right)} \tag{38}$$

where $\mu_1 \geqslant 1$ (depends only on α_0 and α_1) and \bar{e} is the maximum value of the noise. Hence the derivative interval is deduced as follows:

$$\dot{\mathbf{y}} \in [\dot{\mathbf{y}}_{\text{est}} - \varepsilon_1, \ \dot{\mathbf{y}}_{\text{est}} + \varepsilon_1] \tag{39}$$

where $\dot{y}_{est} = z_1$ is the estimate of the first derivative of y.

Proposition. Let us consider e_0 as the error between the estimated variable z_0 and its measured value y. If a second order sliding motion is induced forcing $e_0 = \dot{e}_0 = 0$, then z_1 provides an estimate of \dot{y} according to the first order sliding mode differentiator.

Proof. Let us consider the scalar differential equation $\dot{x}(t) = g(t,x)$ where the measured output y(t) = x(t) in fault free conditions. Let us define a variable $e_0(t) = z_0 - y(t)$, the equations can be rewritten as follows:

$$\begin{cases} \dot{e}_0 = -\alpha_0 \cdot \sqrt{|e_0(t)|} \cdot \operatorname{sign}(e_0(t)) + z_1 - g(t, x) \\ \dot{z}_1 = -\alpha_1 \operatorname{sign}(e_0(t)) \end{cases}$$

$$(40)$$

Let us define a new variable $e_1(t) = z_1(t) - g(t,x)$. Then, (40) can be rewritten as:

$$\begin{cases} \dot{e}_0 = -\alpha_0 \cdot \sqrt{|e_0(t)|} \cdot \operatorname{sign}(e_0(t)) + e_1(t) \\ \dot{e}_1 = -\alpha_1 \operatorname{sign}(e_0(t)) - \dot{g}(t, x) \end{cases}$$

$$(41)$$

If a second order sliding motion is induced forcing $e_0(t) = \dot{e}_0(t) = 0$, then the first equation implies $e_1(t) = 0 \Rightarrow z_1(t) = g(t,x)$. Consequently, z_1 provides an estimate of $\dot{x}(t)$ i.e. $\dot{y}(t)$. \square

2.3. Comparative study

In this paper, a comparison study between three differentiators is performed. The three differentiation methods are as follows: *Moving average differentiator*, the proposed differentiator described above and the Super-Twisting (ST) differentiator proposed by Levant. The latter are not described in this paper and the readers can refer: [43] for the ST differentiator and [49] for the description of moving average differentiator.

2.3.1. Performance indicators

A range of model validation statistical indicators have been used to provide a numerical description of goodness of the derivative estimates. The first performance-indicator chosen is Index of Agreement (IoA) which was developed as a standardized measure of the degree of model prediction error and varies between 0 and 1. A value of 1 indicates a perfect match, and 0 indicates no agreement at all. The index of agreement can detect additive and proportional differences in the observed and simulated means and variances. The IoA is presented under two ratios d_1 and d_2 calculated as follows:

$$d_{1} = 1 - \frac{\sum_{i=1}^{N} |P_{i} - O_{i}|}{\sum_{i=1}^{N} (|P_{i} - O| - |O_{i} - O|)}; \ d_{2} = 1 - \frac{\sum_{i=1}^{N} |P_{i} - O_{i}|^{2}}{\sum_{i=1}^{N} (|P_{i} - O| - |O_{i} - O|)^{2}}$$

$$(42)$$

where N is the number of data points, O_i the observed data points, P_i the predicted data points and O the average of observed data.

Another performance indicator is exploited, namely the *Percentage Variance Accounted For* (VAF). The VAF verifies the correctness of a model by comparing the real output (derivative signal) with the estimated output of the model (derivative estimate). The VAF is calculated as follows:

$$VAF = \left(1 - \frac{\frac{1}{N} \sum_{i=1}^{N} [O_i - P_i]^2}{\frac{1}{N} \sum_{i=1}^{N} [O_i]^2}\right) \times 100 \tag{43}$$

2.3.2. Performance study

In order to assess the accuracy of each differentiator, a sinusoidal signal is used as an input and the results given by the aforementioned indicators are assessed. Different simulations with different noise magnitudes have been performed in order to determine the best differentiator among the three considered ones. In the simulation tests, a reference signal is used as in [49]. The reference signal is a sinusoidal signal $y_{ref} = 1.5 \sin(2\pi f_{eq}t)$. The frequency is fixed to be $f_{eq} = 0.8$ Hz and the sampling time is fixed at $T = 10^{-3}$ s. The analytic time derivative of y_{ref} is used as the standard to compare with the estimations. In order to get the best performance, the differentiator parameters have been tuned after a series of simulations. Fig. 5 shows the reference signal with a noise magnitude e = 0.1 and its derivative using the sliding mode differentiator described in Section 2.2.2.1, the Levant differentiator and the moving average differentiator. Moreover, Table 1 summarizes the

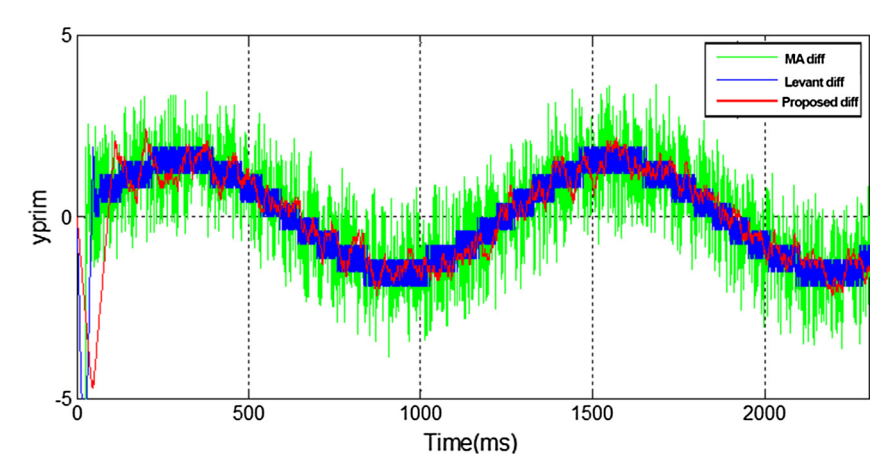


Fig. 5. Given a noisy reference signal (not shown), comparison study between Moving Average differentiator (MA diff, green curve), the derivative using Levant sliding mode differentiator (Levant diff, blue curve) and our proposed sliding mode differentiator (Proposed diff, red curve). (For interpretation of the references to color in this figure legend, the reader is referred to the web version of this article.)

Table 1Performance indicators for noisy signal simulations.

	Performance indicators
Levant differentiator Proposed differentiator Moving average differentiator	$VAF = 67.6333; \ (d_1 = 0.8452 \ and \ d_2 = 0.8883) \\ VAF = 69.4685; \ (d_1 = 0.9389 \ and \ d_2 = 0.9855) \\ VAF = 32.6269; \ (d_1 = 0.6694 \ and \ d_2 = 0.5918) \\$

Table 2Performance indicators for non-noisy signal simulation in Fig. 6.

	Performance indicators
Levant differentiator Proposed differentiator Moving average differentiator	$VAF = 71.1222; \ (d_1 = 0.7252 \ and \ d_2 = 0.6783) \\ VAF = 81,8376; \ (d_1 = 0.8112 \ and \ d_2 = 0.7889) \\ VAF = 92.5148; \ (d_1 = 0.9894 \ and \ d_2 = 0.9218)$

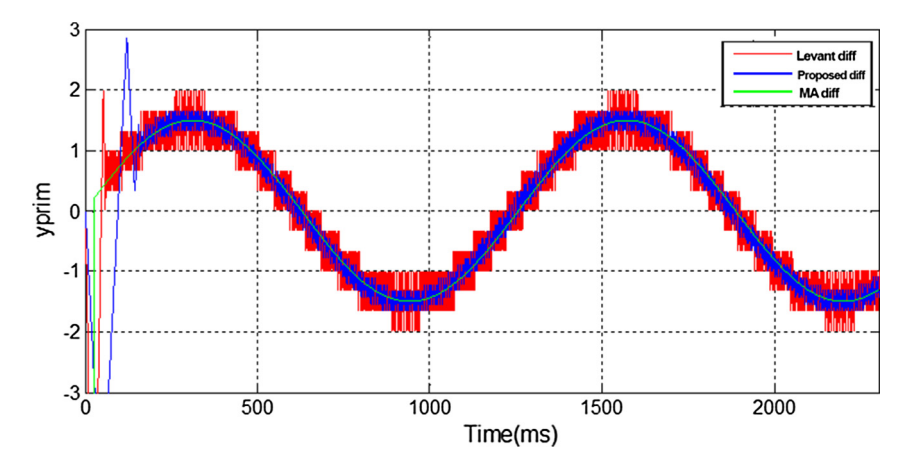


Fig. 6. Given a non-noisy reference signal (not shown), comparative study between Moving Average differentiator (MA diff, green curve), the derivative using Levant sliding mode differentiator (Levant diff, blue curve) and our proposed sliding mode differentiator (Proposed diff, red curve). (For interpretation of the references to color in this figure legend, the reader is referred to the web version of this article.)

performance indicators for each differentiation method for N = 100 simulations with various noise magnitudes (*e* takes values from 0.01 to 0.2) while Table 2 gives the performance indicators when dealing with a non-noisy signal. It is worth noting that the moving average differentiator gives the best results when dealing with non-noisy signal (see Fig. 6). However, in the

presence of the signal noise, the proposed sliding mode differentiator gives better performance (see Fig. 5). Hence, latter is the most suitable differentiator for real applications.

3. Fault detection methodology

Let control/input vector be $\mathbf{U}(t) \in [\mathbf{Se}(t), \mathbf{Sf}(t)]^T$ with $Se(t) \in \mathbb{R}^{N_{Se}}$ and $Sf(t) \in \mathbb{R}^{N_{Sf}}$ as the source of effort and source of flow vectors respectively. Also, nominal system parameter vector $\mathbf{0} \in \mathbb{R}^{N_{\theta}}$ and uncertain parameter vector $[\underline{\mathbf{0}}, \overline{\mathbf{0}}] \in \mathbb{R}^{N_{m}}$ ($N_m \leq N_{\theta}$) are defined. Consider uncertain measurements: uncertain dualized effort detector vector as $[\underline{\mathbf{SSe}}, \overline{\mathbf{SSe}}] \in \mathbb{R}^{N_{SSe}}$ and uncertain dualized flow detector vector as $[\mathbf{SSf}, \overline{\mathbf{SSf}}] \in \mathbb{R}^{N_{SSf}}$.

3.1. FD with respect to uncertain system parameters: I-ARR derivation

First, only uncertain system parameters are considered for I-ARR enabled passive diagnosis (generation of nominal residual and thresholds). Here, the proposed differentiator (see Section 2) is used for signal differentiation and the subsequent residual evaluation. It should be noted that at this stage, measurement uncertainties are not taken into account for threshold generation. Following steps are taken:

- i. Preferred derivative causality is assigned to the nominal model.
- ii. Parametric uncertainties are modelled in interval form and represented on the nominal BG, (see [33]) to obtain uncertain BG.
- iii. The candidate ARRs are generated from 1(0) junction, such that sum of efforts (flows), respectively, is equal to zero, as shown in (44) and (45), where *s* is the sign of the *bond* according to energy convention.
- for 0-junction:

$$\sum s \cdot [\underline{f}, \overline{f}] + \sum Sf + \sum_{i=0}^{i \leq N_m} s_i \cdot MSf : [w_i] = 0$$

$$(44)$$

• for 1-junction:

$$\sum s \cdot [\underline{e}, \overline{e}] + \sum Se + \sum_{i=0}^{i \leq N_m} s_i \cdot MSe : [w_i] = 0$$

$$(45)$$

iv. The unknown effort or flow variables are then eliminated using covering causal paths (following the causal relationships) from unknown variables to known (measured) variables (dualized detectors), to obtain *i*th I-ARR, $[R_{i,l}, R_{i,u}]$. The latter contains only known variables and their derivatives (c.f. (46)).

$$[R_{i,l}, R_{i,u}] : \Psi_i \theta_n, [\underline{\theta}, \overline{\theta}], [w_i], \sum Se, \sum Sf(, SSe(t), SSe(t), SSe(t), SSF(t), SSf($$

v. I-ARR $[R_{i,l}, R_{i,u}]$ is composed of point valued function $\Psi_{i,1}$ and interval valued part identified as interval function $\Psi_{i,2}$ as shown in (47)–(49).

$$[R_{i,l}(t), R_{i,u}(t)] : Ir_{i,n}(t) + [B_{i,l}(t), B_{i,u}(t)]$$

$$(47)$$

$$Ir_{i,n}(t) = \Psi_{i,1}(\theta_{\mathbf{n}}, \mathbf{SSe}(t), \mathbf{SSf}(t), \sum Se, \sum Sf, \widehat{\mathbf{SSe}(\mathbf{t})}, \widehat{\mathbf{SSf}(\mathbf{t})})$$

$$\tag{48}$$

$$[B_{i,l}(t), B_{i,u}(t)] = \Psi_{i,2}([\underline{\theta}, \overline{\theta}], [\delta_{\theta}, \overline{\delta_{\theta}}], SSe(t), SSf(t), [-\varepsilon, \varepsilon])$$

$$(49)$$

vi. As seen in (48), the nominal part is formed by point valued function $\Psi_{i,1}$, which is sensitive to nominal values of the parameters, measurements, and estimate of the measurement derivatives. The proposed sliding mode differentiator (Section 2.2.2) is exploited for estimation of the flow (or effort) derivative as (c.f. (38) and (39)),

$$SS\dot{f}_{j}(t) \in \left[\widehat{SSf_{j}(t)} - \varepsilon_{SSf_{j}}, SS\dot{f_{j}(t)}\right] + \varepsilon_{SSf_{j}}$$

$$SS\dot{f}_{j}(t) \in SS\dot{f}_{j}(t) + [-\varepsilon_{SSf_{j}}, +\varepsilon_{SSf_{j}}]$$
(50)

The interval valued part identified as interval function $\Psi_{i,2}$ sensitive to interval valued uncertainties, measurements and vector of derivative uncertainty intervals $[-\varepsilon, \varepsilon]$ (cf. (49)).

3.1.1. Evaluation of URIF range

- vii. Point valued arguments and arithmetic operators of URIF $\Psi_{i,2}$ are replaced by the corresponding interval arguments and interval arithmetic operators [29,33]. URIF $\Psi_{i,2}$ is expressed as finite sequence of interval arithmetic operations. viii. URIF range $[B_{i,l}(t), B_{i,u}(t)]$ is obtained using Interval Arithmetic and following conditions are achieved [29,33]:
- Under nominal conditions (see [33] for proof),

$$-Ir_{i,n}(t) \in [B_{i,l}(t), B_{i,u}(t)] \tag{51}$$

• Under Parametric Fault:

$$-Ir_{i,n}(t) \notin [B_{i,l}(t), B_{i,u}(t)] \tag{52}$$

3.2. FD with respect to uncertain system measurements: derivation of feasible conditions

While the previous section considered uncertain parameters, this section exploits FME to develop FD method with respect to uncertain measurements. To that end, nominal residuals associated with each of the I-ARRs derived previously, are considered bounded between the interval limits provided by their respective URIF range (see Section 3.1).

- ix. The set of *nominal residuals* $Ir_{i,n}(t)$ for $i = 1, 2 ... N^{IARR}$ where N^{IARR} are the total number of I-ARRs (c.f. (53)), are considered as a system of linear inequalities: *System S1* (see (53)), bounded by interval limits given by URIF range evaluation, as obtained previously in (51).
- x. Moreover, each of the uncertain measurements are considered bounded: System S2 (54).

FME method is applied over *System S*0, such that upper and lower bounds over each of the measurements are found in terms of known system parameters and measurement uncertainties.

- v. The parametric faults are assessed with respect to *System S*1 by verifying the contentment of nominal residual inside the interval limits (thresholds) provided by the respective URIF ranges.
- vi. Measurement faults are assessed using the conditions provided by FME over system S0.

4. Study on mechatronic system

The mechatronic Torsion Bar 1.0 system has already been the subject of simulation-experimental study in [33], where only uncertain parameters are taken into consideration. Therein, measurement uncertainties have not been taken into account. In this paper, in order to maintain coherence with previous work, authors have maintained the same notations and system variable designations. This paper does not detail the system functioning and BG models. Instead readers are referred to [33,45,46] for description of the latter. The schematic model of the system and nominal BG model is presented in Appendix A. Table 3 provides the details of various system parameters and variables.

Moreover, in this paper, it has been assumed that elastic force (spring action) manifesting in the torsion bar is measured by a force sensor. In reality, this translates to the usage of force sensors (like strain gauges) for stress/strain measurement. This is done to prevent the problems arising due to initial conditions and presence of an integral term. This assumption of the presence of a force sensor (*Df*: F, see Fig. A.2) is made to demonstrate the method successfully. MATLAB 2011a® and Simulink2011a® have been used for simulation purposes. The interval valued functions have been written in *Matlab Function Block* in Simulink and integrated with INTLAB® [47] to execute interval calculations during simulation.

Fig. 7 shows the system response obtained by simulation of nominal BG (see Fig. A.2) under nominal conditions. The system is considered **operating in feedback closed loop (Proportional-Integral (PI) control)**. The motor velocity ω_m is

Table 3System parameters and variables.

Parameter θ	Designation	Nominal value θ_n	Multiplicative uncertainty $\left[\underline{\delta_{\theta}}, \overline{\delta_{\theta}}\right]$
ks	Spring constant of the shaft	1.786 N·m/rad	[-0.1,0.1]
b_s	Damping coefficient of shaft	$5.11 \times 10^{-4} \text{ N} \cdot \text{m/rad}$	[-0.1, 0.1]
k_m	Torque constant	$3.89 \times 10^{-4} \text{ N} \cdot \text{m/A}$	=
k_{belt}	Teeth ratio (motor disk and motor shaft)	3.75	-
La	Rotor inductance	$1.34\times10^{-3}\;\text{H}$	-
Ra	Rotor resistance	1.23 Ω	-
Jm	Rotor inertia	$6.76 \times 10^{-6} \text{ kg} \cdot \text{m}^2/\text{rad}$	[-0.2, 0.2]
f_m	Motor friction coefficient	$2 \times 10^{-6} \text{N} \cdot \text{m} \cdot \text{s/rad}$	[0,0.2]
J_{Md}	Motor disk rotational inertia	$9.07 \times 10^{-4} \text{ kg m}^2/\text{rad}$	[-0.1, 0.1]
b_{Md}	Viscous friction in motor disk	$5.025 \times 10^{-3} \mathrm{N \cdot m \cdot s/rad}$	[-0.2, 0.2]
J_{Id}	Load disk rotational inertia	$1.37 \times 10^{-3} \text{ kg} \cdot \text{m}^2/\text{rad}$	[-0.2, 0.2]
b_{Ld}	Viscous friction in load disk	$2.5 \times 10^{-5} \text{N} \cdot \text{m} \cdot \text{s/rad}$	[-0.2, 0.2]
$SSf_1:\omega_m$	Motor velocity measurement	-	- -
$SSf_2:\omega_{Ld}$	Load disk velocity measurement	-	-
SSe:F	Measurement of Elastic Force in the Torsion Bar	_	_

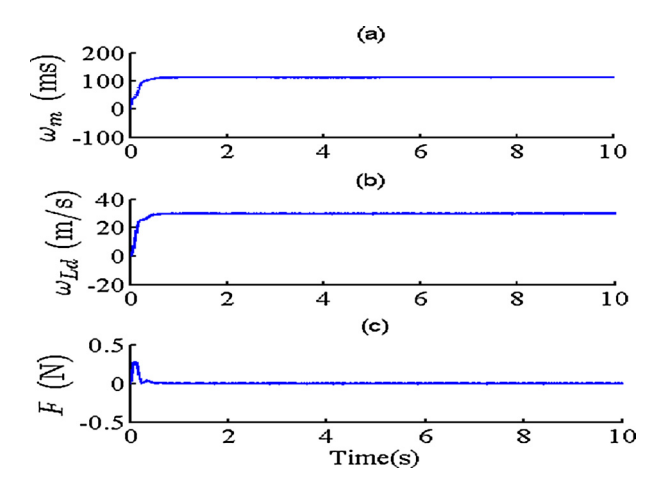


Fig. 7. System response under nominal conditions (a) motor velocity measurement, (b) load disk velocity and (c) elastic force in torsion bar.

controlled at reference $\omega_{m,ref} = 112.5 rad/s$ so that motor disk velocity ω_{Md} is regulated to $\omega_{Md,ref} = \omega_{m,ref}/k_{belt} = 30 \text{ rad/s}$. Zero mean Gaussian noise is added to sensor (measurement) outputs.

4.1. Parametric FD module: I-ARRs and Robust thresholds

The parametric faults are detected using I-ARRs which generate nominal residuals and interval valued thresholds. The methodology detailed in Section 3.1 is followed.

- i. Taking uncertain system parameters into consideration, the uncertain BG of the monitorable part of the system is constructed in preferred derivative causality (see Fig. A.3). All the sensors are dualized and impose corresponding flows/efforts as $SSf_1: \omega_m, SSf_2: \omega_{Id}, SSe: F$.
- ii. Two I-ARRs are derived from the junctions $\mathbf{1}_1$ and $\mathbf{1}_2$ (see Fig. A.3) as given in (55) and (59) respectively.

From Junction 1₁:

$$\begin{split} & \left[\underline{R}, \overline{R}\right]_{1} = \tau_{PI} - (J_{m,n} \dot{\omega}_{m} + \left[\underline{\delta_{J_{m}}}, \overline{\delta_{J_{m}}}\right] J_{m,n} \dot{\omega}_{m}) - (f_{m,n} \omega_{m} + \left[\underline{\delta_{f_{m}}}, \overline{\delta_{f_{m}}}\right] f_{m,n} \cdot \omega_{m}) - (1/k_{belt}) ((J_{Md,n} (\dot{\omega}_{m}/k_{belt})) \\ & + \left[\delta_{J_{Md}}, \overline{\delta_{J_{Md}}}\right] J_{Md,n} (\dot{\omega}_{m}/k_{belt})) + (b_{Md,n} (\omega_{m}/k_{belt}) + \left[\delta_{b_{Md}}, \overline{\delta_{b_{Md}}}\right] b_{Md,n} \cdot (\omega_{m}/k_{belt})) + SSe : F) \end{split} \tag{55}$$

The first I-ARR is sensitive to measurements SSf: ω_m and their first order derivatives. The latter is estimated using the proposed sliding mode differentiator (see Section 2.2.2) as,

$$\dot{\omega}_{m} \in \left[\widehat{\omega}_{m} - \varepsilon_{\omega_{m}}, \widehat{\omega}_{m} + \varepsilon_{\omega_{m}}\right]
\dot{\omega}_{m} = \widehat{\omega}_{m} + \left[\varepsilon_{\omega_{m}}, + \varepsilon_{\omega_{m}}\right]$$
(56)

Then, the nominal part Ir_1 and interval valued part (URIF) can be obtained as,

$$Ir_{1,n}(t) = \tau_{in} - J_{m,n}\widehat{\dot{\omega}_m} - f_{m,n}\omega_m - \frac{1}{k_{belt}} \left(J_{Md,n} \frac{\widehat{\dot{\omega}_m}}{k_{belt}} + b_{Md,n} \frac{\omega_m}{k_{belt}} + SSe : F \right)$$

$$(57)$$

$$[B(t)_{1,l}, B(t)_{1,u}] = \left(\left[\underline{\delta_{J_m}}, \overline{\delta_{J_m}} \right] J_{m,n} \widehat{\omega_m} \right) - \left[\underline{J_m}, \overline{J_m} \right] \left[-\varepsilon_{\omega_m}, +\varepsilon_{\omega_m} \right] - \left(\left[\underline{\delta_{f_m}}, \overline{\delta_{f_m}} \right] f_{m,n} \cdot \omega_m \right) - \frac{1}{k_{belt}} \left(\left[\underline{\delta_{J_{Md}}}, \overline{\delta_{J_{Md}}} \right] J_{Md,n} \widehat{\frac{\dot{\omega}_m}{k_{belt}}} + \left[\underline{J_{Md}}, \overline{J_{Md}} \right] J_{Md,n} \widehat{\frac{(-\varepsilon_{\omega_m}, +\varepsilon_{\omega_m}]}{k_{belt}}} + \left[\underline{\delta_{b_{Md}}}, \overline{\delta_{b_{Md}}}, \overline{\delta_{b_{Md}}} \right] b_{Md,n} \widehat{\frac{\omega_m}{k_{belt}}} \right)$$

$$(58)$$

Similarly, energetic assessment at Junction 12 gives:

$$\left[\underline{R},\overline{R}\right]_{2} = F - J_{Ld,n}\dot{\omega}_{Ld} - b_{Ld,n}\omega_{Ld} - \left[\underline{\delta_{J_{Ld}}},\overline{\delta_{J_{Ld}}}\right]J_{Ld,n}\dot{\omega}_{Ld} - \left[\underline{\delta_{b_{Ld}}},\overline{\delta_{b_{Ld}}}\right]b_{Ld,n}\omega_{Ld}$$

$$(59)$$

The load disk velocity is differentiated using the sliding mode differentiator and the derivative is estimated as,

$$\dot{\omega}_{Ld} \in \left[\widehat{\dot{\omega}_{Ld}} - \varepsilon_{\omega_{Ld}}, \widehat{\dot{\omega}_{Ld}} + \varepsilon_{\omega_{Ld}}\right] \text{ or, } \dot{\omega}_{Ld} = \widehat{\dot{\omega}_{Ld}} + \left[-\varepsilon_{\omega_{Ld}}, +\varepsilon_{\omega_{Ld}}\right]$$

$$(60)$$

Then, the nominal part Ir2 and associated URIF can be obtained as,

$$Ir_{2,n}(t) = F - J_{Ld,n}\widehat{\dot{\omega}_{Ld}} - b_{Ld,n}\omega_{Ld}$$

$$\tag{61}$$

$$[B(t)_{2,l}, B(t)_{2,u}] = -\left[\underline{\delta_{J_{Ld}}}, \overline{\delta_{J_{Ld}}}\right] J_{Ld,n} \widehat{\omega_{Ld}} - [\underline{J_{Ld}}, \overline{J_{Ld}}] [-\varepsilon_{\omega_{Ld}}, +\varepsilon_{\omega_{Ld}}] - \left[\delta_{b_{Ld}}, \overline{\delta_{b_{Ld}}}\right] b_{Ld,n} \omega_{Ld}$$

$$(62)$$

It should be noted that electrical torque $MSe: \tau_{Pl}$ is a PI controlled input to the monitorable part of the system; it is given as:

$$MSe: \tau_{Pl} = k_m \cdot i_m = k_m \cdot \frac{(U_{Pl} - k_m \cdot \omega_m)}{Ra} \left(1 - e^{-(Ra/La) \times t} \right)$$

$$\tag{63}$$

where U_{Pl} is the PI controlled voltage input and i_m is the motor-stator current.

4.2. Measurement FD module

A measurement signal is inevitably corrupted with noise. The noise manifesting in the signal often masks the measurement deviation/fault. Detection of abrupt changes in sensor measurements, modelling sensor drift and measurement bias/tolerance-intervals are some of the significant issues that invoke the need for modelling measurement uncertainties.

4.2.1. Modelling system measurement uncertainty

Consider a measurement signal y(t) at time t. The noise is assumed to be normally-distributed Gaussian in nature, or

$$p(y(t)) = \frac{1}{\sigma_{\overline{y(t)}}\sqrt{2\pi}} \exp\left(-(y(t) - \bar{y}(t))^2/2\sigma_{\overline{y(t)}}^2\right)$$
(64)

where p denotes the probability density function, $\sigma_{\overline{y(t)}}$ is the standard deviation and $\overline{y}(t)$ is the smoothed mean of the signal in a running window of previous W signals. Common methods for signal smoothening include usage of moving median filters, Finite Impulse Response (FIR) filters, etc. In this paper, a sliding window of previous W estimates is considered for generation of smoothed (mean) signal as,

$$\overline{y}(t) = \begin{cases} \frac{1}{W+1} \sum_{w=0}^{l=W} y(t-w) & \text{if } t \geqslant W \\ y(t-w) & \text{if } t < W \end{cases}$$

$$(65)$$

In this paper, uncertainty interval over a measurement is modelled by taking into account the noise variance over the mean measurement. The measurement signal is bounded as shown in (66) which accounts for 99.7% of signal values around the smoothed mean $\overline{y}(t)$. Denoting $\overline{y}(t) - 3\sigma_{\overline{y(t)}} \equiv y(t)_l$ and $\overline{y}(t) + 3\sigma_{\overline{y(t)}} \equiv y(t)_u$, the signal is bounded as shown in (67).

$$\bar{y}(t) - 3\sigma_{\overline{y(t)}} < y(t) < \bar{y}(t) + 3\sigma_{\overline{y(t)}}$$

$$\tag{66}$$

$$y_1(t) < y(t) < y_n(t)$$
 (67)

Thus, following the same notation, the speed and force measurements from the sensors are considered as,

$$\omega_{m,l}(t) < \omega_{m}(t) < \omega_{m,u}(t)
\omega_{Ld,l}(t) < \omega_{Ld}(t) < \omega_{Ld,u}(t)
F_{l}(t) < F_{l}(t) < F_{u}(t)$$
(68)

It should be noted that sensor-tolerance intervals can also be treated in the similar fashion to model the associated uncertainty.

4.2.2. Determination of feasible conditions on uncertain measurements

The measurement bounds considered in (68) do not take into account the influence of parametric faults over sensor measurements. In other words, the measurement bounds considered in (68) are sensitive to changes in measurements only; as such, they remain sensitive to false alarms caused by changes in measurements due to parametric faults/deviations. Then, as discussed in Section 3.2, FME technique is employed to obtain feasible conditions (bounds) over measurements while the parametric deviations/faults are also taken into account.

System S0 considered for application of FME is shown in (69). System S1 is constituted by two nominal residuals derived in (57) and (61), which remain bounded by their respective URIF ranges (58) and (62), under null parametric faults (nominal conditions). System S2 comprises of set of constraints formed by relations considered in (68).

$$System S0 \begin{cases} System S1 \begin{cases} B_{1,l}(t) \leqslant \left(\tau_{in} - J_{m,n}\widehat{\dot{\omega}_{m}} - f_{m,n}\omega_{m} - \frac{1}{k_{belt}}\left(J_{Md,n}\frac{\widehat{\dot{\omega}_{m}}}{k_{belt}} + b_{Md,n}\frac{\omega_{m}}{k_{belt}} + SSe:F\right)\right) \leqslant B_{1,u}(t) \\ B_{2,l}(t) \leqslant (F - J_{Ld,n}\widehat{\dot{\omega}_{Ld}} - b_{Ld,n}\omega_{Ld}) \leqslant B_{2,u}(t) \\ System S2 \begin{cases} \omega_{m,l}(t) < \omega_{m}(t) < \omega_{m,u}(t) \\ \omega_{Ld,l}(t) < \omega_{Ld}(t) < \omega_{Ld,u}(t) \\ F_{l}(t) < F(t) < F_{u}(t) \end{cases} \end{cases}$$

$$(69)$$

FME method (see Section 2.2.1) is applied over *System SO*. In fact it can be observed that the set of inequalities described here in (69) are analogous to the one considered in Example 2 (c.f. (15)–(20)). The correspondence is clear from the relations given in (70) and (71).

$$\begin{cases} r_{1} = -Ir_{1,n}; \\ r_{2} = -Ir_{2,n}; \end{cases} \begin{cases} x_{1} = SSe : \omega_{m}(t) \\ x_{2} = SSe : F(t) \\ x_{3} = SSf : \omega_{Ld}(t) \end{cases} \begin{cases} a_{2} = -1; \\ b_{2} = b_{Ld,n}\omega_{Ld}; \\ c_{2} = J_{Ld,n}\widehat{\omega}_{Ld} \end{cases} \begin{cases} a_{1} = f_{m,n} + \frac{b_{Md,n}}{k_{belt}^{2}}; \\ b_{1} = \frac{1}{k_{belt}}; \\ c_{1} = \tau_{in} - J_{m,n}\widehat{\omega}_{m} - J_{Md,n}\widehat{k_{belt}^{2}} \end{cases}$$
 (70)

$$\begin{cases}
q_{1} = B_{1,l}(t), q_{2} = B_{1,u}(t) \\
l_{1} = B_{2,l}(t), l_{2} = B_{2,u}(t)
\end{cases}
\begin{cases}
i_{1} = \omega_{m,l}(t), i_{2} = \omega_{m,u}(t) \\
j_{1} = F_{l}(t); j_{2} = F_{u}(t) \\
k_{1} = \omega_{Ld,l}(t); k_{2} = \omega_{Ld,u}(t)
\end{cases} (71)$$

Thus, FME can be applied in a manner similar to the one shown for Example 2, with the values of coefficients and variables as shown in (70) and (71). The latter leads to a feasible condition and set of upper and lower bounds on measurements, as obtained in (31), (33) and (34). Here, the feasible conditions have not been derived explicitly due to their obvious correspondence with Example 2; instead, they are denoted as:

$$\underline{\omega_{m,FME}} \leqslant \omega_m \leqslant \overline{\omega_{m,FME}}
\underline{\omega_{Ld,FME}} \leqslant \omega_{Ld} \leqslant \overline{\omega_{Ld,FME}}
\underline{F_{FME}} \leqslant F \leqslant \overline{F_{FME}}$$
(72)

4.3. Fault detection

A step input voltage of 220 V is given to the system. Fig. 8 shows the nominal residuals and interval valued thresholds under nominal system conditions (without parametric, measurement faults). Evaluation of I-ARRs involves the usage of proposed sliding-mode differentiator, such that derivatives $\dot{\omega}_m$ and $\dot{\omega}_{Ld}$ are estimated as shown in (56) and (60) respectively. As seen in Fig. 8, the nominal residuals are well contained within respective URIF bounds (thresholds). Here, the Lipschitz's

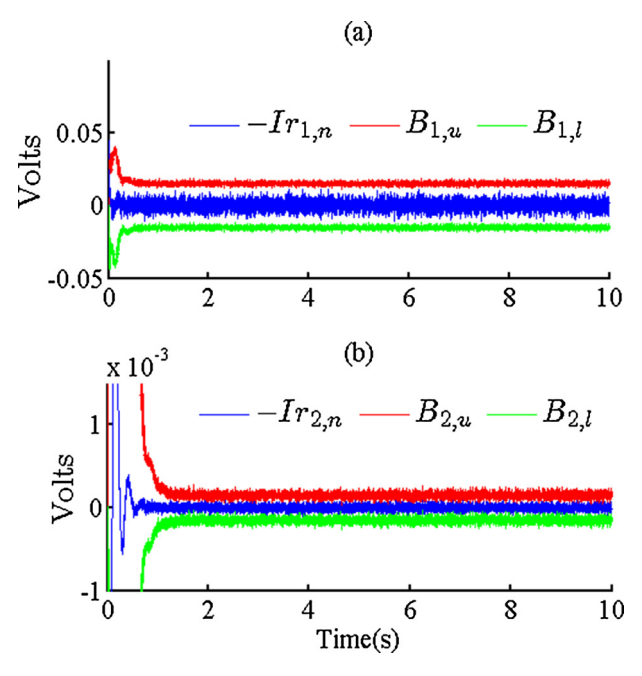


Fig. 8. I-ARRs under nominal conditions with sliding mode differentiator (a) the nominal part Ir_1 and associated URIF and (b) nominal part Ir_2 and associated URIF.

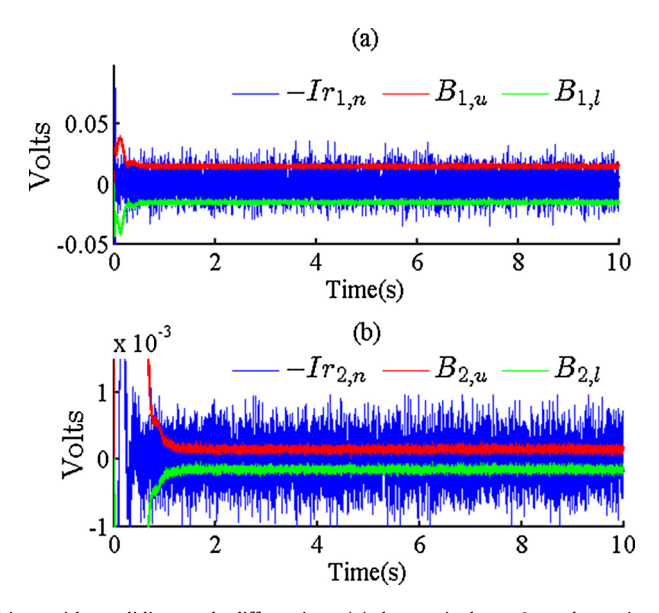


Fig. 9. I-ARRs under nominal conditions without sliding mode differentiator (a) the nominal part Ir_1 and associated URIF and (b) nominal part Ir_2 and associated URIF.

constants L_{ω_m} , $L_{\omega_{Ld}}$ are chosen in such a way that signal derivatives are estimated with maximum VAP (c.f. (43)) and e_{ω_m} , $e_{\omega_{Ld}}$ are the maximum value of the Gaussian noise added to the ω_m and ω_{Ld} measurements respectively.

$$\varepsilon_{\omega_{m}} = \mu_{\omega_{m}} \sqrt{L_{\omega_{m}}} \cdot (e_{\omega_{m}})^{(-\frac{1}{2})}; \quad \mu_{\omega_{m}} = 1; \ L_{\omega_{m}} = 0.0025; \ e_{\omega_{m}} = 0.001$$

$$\varepsilon_{\omega_{td}} = \mu_{\omega_{td}} \sqrt{L_{\omega_{td}}} \cdot (e_{\omega_{td}})^{(-\frac{1}{2})}; \quad \mu_{\omega_{td}} = 1; \ L_{\omega_{td}} = 0.0031; \ e_{\omega_{td}} = 0.0001$$
(73)

Fig. 9 shows the nominal residuals without sliding mode differentiator. Clearly, it is corrupted with noise due to signal differentiation which subsequently leads to an increased risk of false alarms or missed alarms. Fig. 10 shows the sensor measurements bounded by their respective FME derived limits (c.f. (72)). The width of the sliding windows (c.f. (65)) *W* is 100 samples.

4.3.1. Parametric faults

In this section, only parametric faults are introduced in the system. Fig. 11 shows a 20% deviation of motor disk friction coefficient over its nominal value. The URIF bounds consider 10% parametric deviation as uncertainty (see Table 3). Thus, the injected deviation is detected as a fault. Similarly, Fig. 12 considers 30% deviation on load disk friction. The URIFs consider 20% parametric deviation as inherent uncertainty. As seen in Figs. 11 and 12, the injected deviations are detected as fault when the nominal residual(s) go outside their thresholds (URIF bounds).

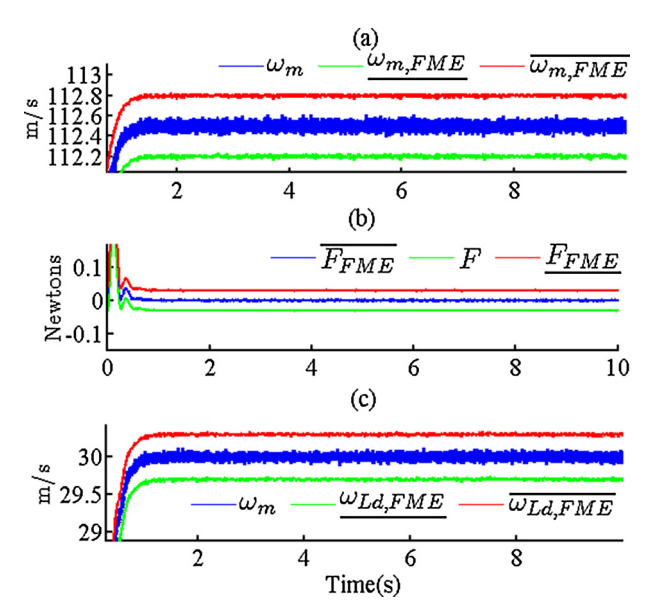


Fig. 10. Measurements under nominal conditions bounded by FME enabled bounds (a) motor velocity measurement, (b) elastic force in torsion bar and (c) load disk velocity.

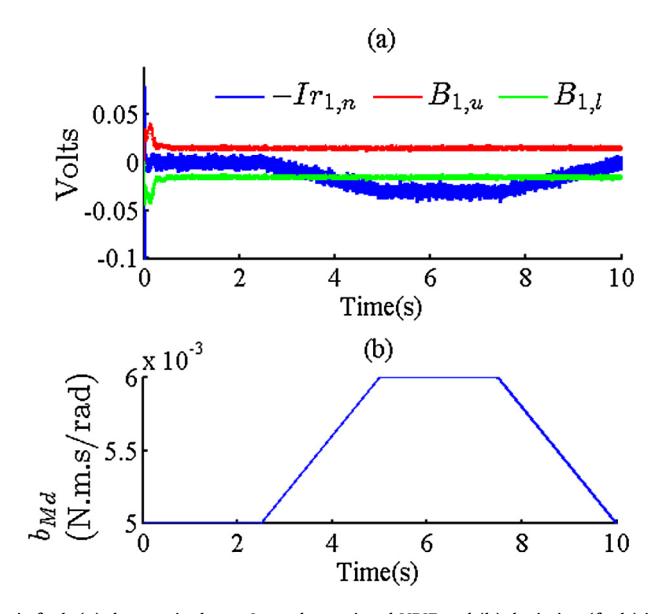


Fig. 11. I-ARR under parametric fault (a) the nominal part Ir₁ and associated URIF and (b) deviation (fault) injected in motor disk friction.

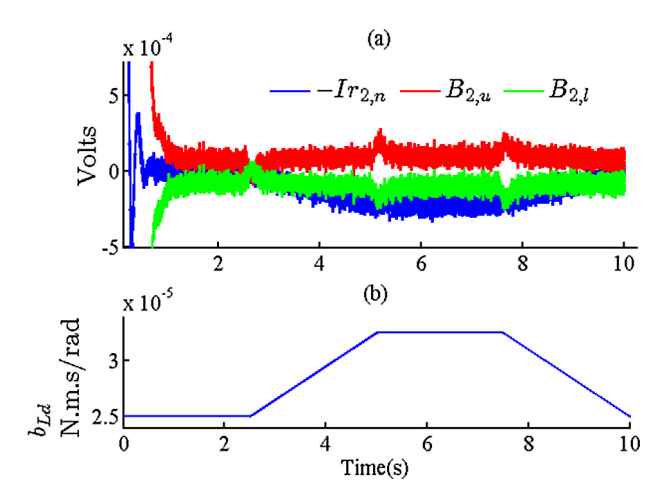


Fig. 12. I-ARR under parametric fault (a) the nominal part Ir₂ and associated URIF and (b) deviation (fault) injected in load disk friction.

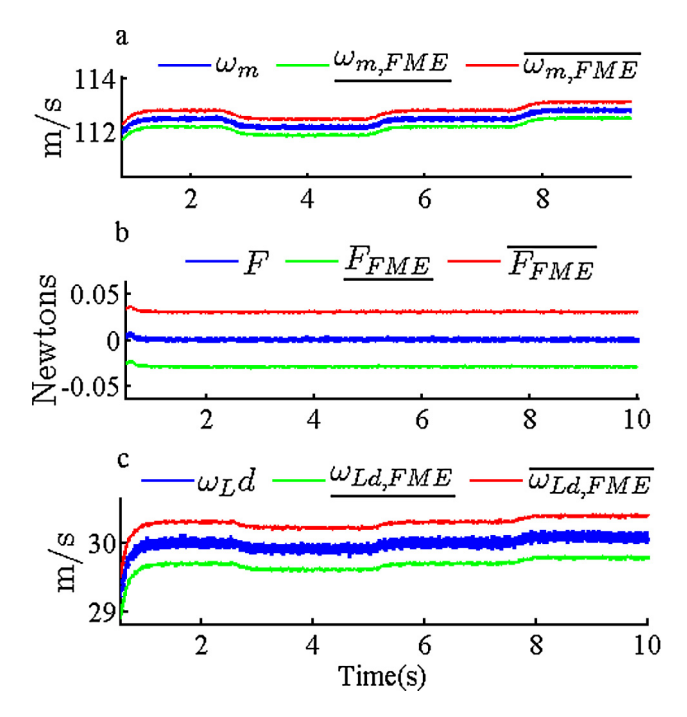


Fig. 13. System measurements with parametric faults bounded by FME derived bounds (a) motor velocity measurement, (b) elastic force in torsion bar and (c) load disk velocity.

It should be noted that there have been no measurement faults injections yet. As such, it is interesting to observe the system measurement(s) profile(s). Fig. 13 shows the sensor measurements bounded by FME derived bounds (envelopes). With only parametric faults, system S1 (c.f. (69) has no solution in faulty regime. Therein, FME bounds (c.f. (72)) on measurements are influenced by $\pm 3\sigma$ bounds (c.f. (68)).

4.3.2. Measurement faults

Abrupt change in speed measurements are introduced in form of short pulses as shown in Fig. 14. Such faults can be of various types. In this paper, only abrupt changes are considered. As seen in Fig. 14, abrupt faults are successfully detected when the measurement signal goes out of the FME derived bounds. Sliding window length (W = 100 samples here) directly influences the smoothed signal quality. Larger W implies larger lag introduced into the smoothed signal. While a larger lag is helpful in detection of abrupt changes, it may lead to non-containment of signal within FME bounds during transient

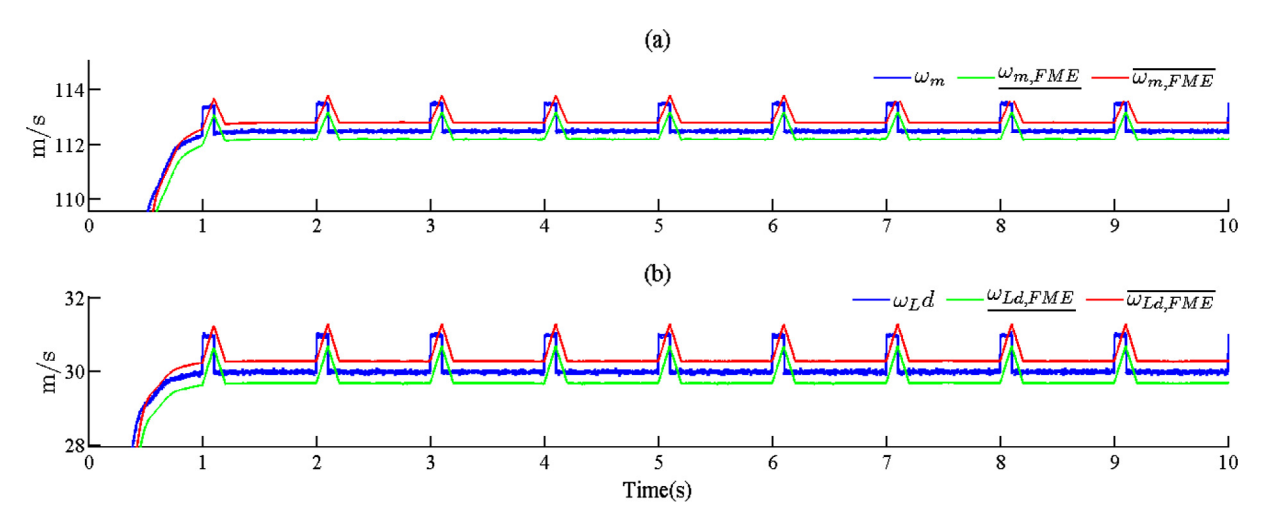


Fig. 14. System measurements with abrupt faults (a) motor velocity measurement and (b) load disk velocity.

regimes. Moreover, W determines the moving variance and $\pm 3\sigma$ bounds. Thus, a trade-off must be achieved between fault detection and the transient regime performance.

An abrupt change can be distinguished against gradual degradation using qualitative/quantitative trend analysis techniques [40], hypothesis testing, outlier identification [9,48], etc. These methods will be applied in future works.

5. Conclusions

- 1. The FD method presented in this paper shows that the proposed first-order sliding mode differentiator can be successfully integrated within the framework of I-ARRs based fault diagnosis. Optimal estimations of measurement signal derivatives sensitive to I-ARRs, lead to noise reduction in nominal residual evaluations. This is helpful in insuring their appropriate containment within the interval valued thresholds. This considerably reduces the possibilities of false alarms and missed alarms. Moreover, the associated interval-valued accuracy bounds can be used for threshold generation by including it as an interval variable. The latter lead to successful detection of parametric faults. Sensitivity analysis is usually helpful in quantitative assessment of parametric deviation over residual change. The latter has not been studied in this paper and can be referred in [26]. Moreover, residual based fault isolability problem [14] has not been studied in the context of I-ARR enabled diagnosis. This will be explored in future works.
- 2. The comparative study has shown that our differentiator leads to better estimation performance when compared with existing differentiators. Moreover, a better performance can be obtained with tunable Lipschitz's constant.
- 3. In future, this framework will be used as FD module for diagnostics and fault prognostics. As such, this work along with work presented in [33] shall form the basic building block of integrated health monitoring architecture (diagnostics and prognostics).
- 4. The FME technique has been integrated suitably within the I-ARR based diagnosis such that measurement faults can be detected successfully. In this paper, only abrupt sensor faults are considered. In future, various other phenomena like sensor drift, sensor bias will be considered exploiting the same framework.
- 5. Exploitation of FME technique for FD purposes creates the possibilities for other powerful optimization techniques such as advanced convex optimization methods and set membership based techniques for similar objectives. Authors are enthusiastic to integrate such advanced techniques for integrated system supervision.

Acknowledgments

This work has been fulfilled within the framework of the DeGaDeCom project. The authors would like to thank the University of Angers for providing financial support under this project.

Appendix A

See Figs. A.1-A.3.

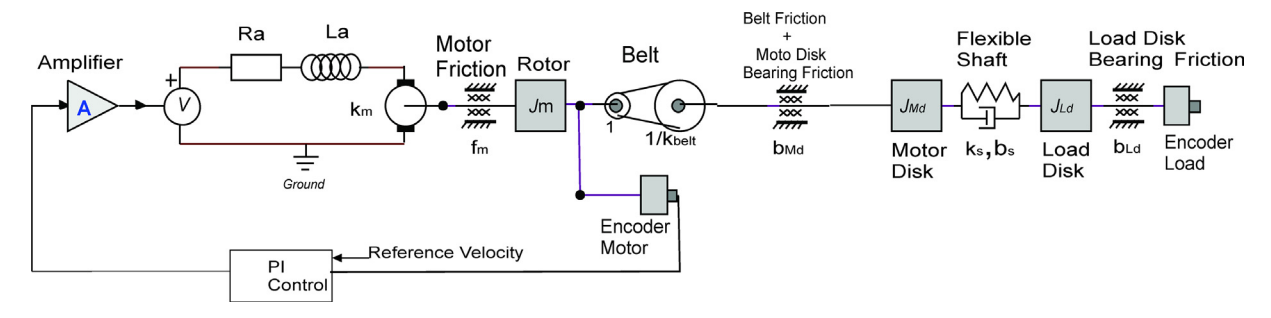


Fig. A.1. Schematic model of the mechatronic system.

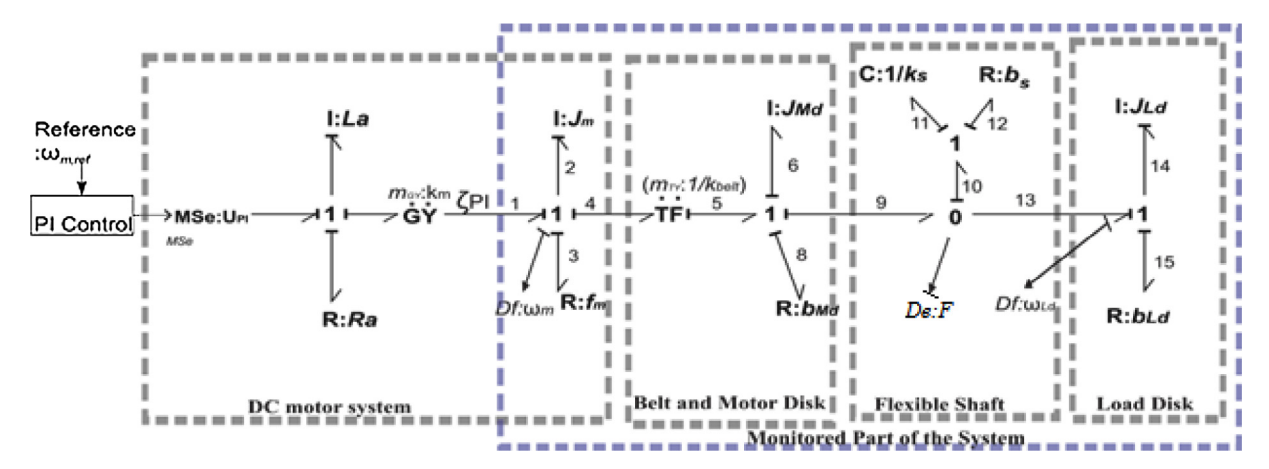


Fig. A.2. Bond graph model (preferred integral causality) of the nominal system.

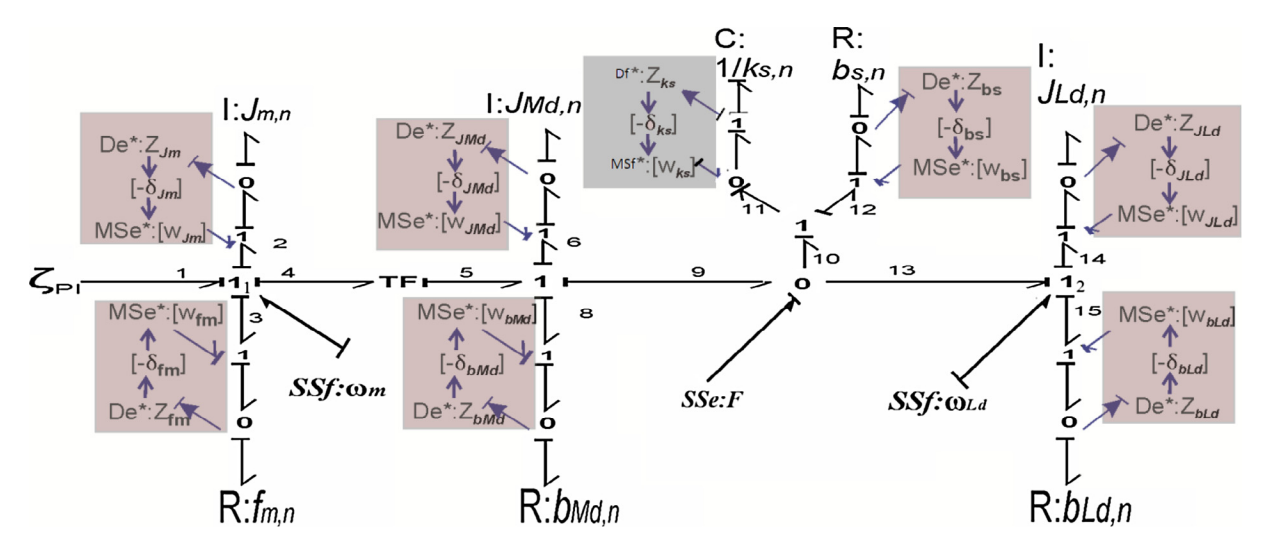


Fig. A.3. Bond graph model of monitorable part in preferred derivative causality with parametric uncertainties as intervals.

Appendix B. Supplementary material

Supplementary data associated with this article can be found, in the online version, at $\frac{\text{http:}}{\text{dx.doi.org}} = \frac{10.1016}{\text{j.ymssp.}} = \frac{2017.02.022}{\text{dx.doi.org}} = \frac{10.1016}{\text{j.ymssp.}} = \frac{10.1016}{\text{l.ymssp.}} = \frac{10.1016}{\text{l.ymssp.}}$

References

- [1] E.Y. Chow, A.S. Willsky, Analytical redundancy and the design of robust failure detection systems, IEEE Trans. Automatic Control 29 (1984) 603–614.
- [2] P. Beckerle, H. Schaede, N. Butzek, S. Rinderknecht, Balancing filters: an approach to improve model-based fault diagnosis based on parity equations, Mech. Syst. Signal Process. 29 (2012) 137–147.
- [3] M. Blanke, M. Kinnaert, J. Lunze, M. Staroswiecki, J. Schrder, Diagnosis and Fault-Tolerant Control, Springer Publishing Company Incorporated, 2010.
- [4] R. Isermann, Model-based fault-detection and diagnosis-status and applications, Annu. Rev. Control 29 (2005) 71-85.
- [5] M.A. Demetriou, Using unknown input observers for robust adaptive fault detection in vector second-order systems, Mech. Syst. Signal Process. 19 (2005) 291–309.
- [6] Y. Wang, J. Xiang, R. Markert, M. Liang, Spectral kurtosis for fault detection, diagnosis and prognostics of rotating machines: a review with applications, Mech. Syst. Signal Process. 66–67 (2016) 679–698.
- [7] J. Chen, R.J. Patton, Robust Model-Based Fault Diagnosis for Dynamic Systems, Springer Science & Business Media, 2012.
- [8] B.O. Bouamama, G. Biswas, R. Loureiro, R. Merzouki, Graphical methods for diagnosis of dynamic systems: review, Annu. Rev. Control 38 (2014) 199–219.
- [9] V. Venkatasubramanian, R. Rengaswamy, S.N. Kavuri, K. Yin, A review of process fault detection and diagnosis, Comput. Chem. Eng. 27 (2003) 327–346.
- [10] V. Venkatasubramanian, R. Rengaswamy, S.N. Kavuri, A review of process fault detection and diagnosis: Part II: qualitative models and search strategies, Comput. Chem. Eng. 27 (2003) 313–326.
- [11] V. Venkatasubramanian, R. Rengaswamy, S.N. Kavuri, K. Yin, A review of process fault detection and diagnosis: Part III: process history based methods, Comput. Chem. Eng. 27 (2003) 327–346.
- [12] H. Paynter, Analysis and Design of Engineering Systems, M.I.T. Press, 1961.
- [13] M. Tagina, J.P. Cassar, G. Dauphin-Tangy, M. Staroswiecki, Monitoring Of Systems Modelled By Bond Graph, in: ICBGM'95, International Conference on Bond Graph Modeling Las Vegas, 1995, pp. 275–280.
- [14] K. Medjaher, A.K. Samantaray, B. Ould Bouamama, M. Staroswiecki, Supervision of an industrial steam generator. Part II: online implementation, Control Eng. Pract. 14 (2006) 85–96.
- [15] N. Chatti, B. Ould-Bouamama, A.-L. Gehin, R. Merzouki, Signed bond graph for multiple faults diagnosis, Eng. Appl. Artif. Intell. 36 (2014) 134–147.
- [16] R. Merzouki, K. Medjaher, M.A. Djeziri, B. Ould-Bouamama, Backlash fault detection in mechatronic system, Mechatronics 17 (2007) 299-310.
- [17] G. Niu, Y. Zhao, M. Defoort, M. Pecht, Fault diagnosis of locomotive electro-pneumatic brake through uncertain bond graph modeling and robust online monitoring, Mech. Syst. Signal Process. 50–51 (2015) 676–691.
- [18] N. Chatti, A. Gehin, B. Ould-Bouamama, R. Merzouki, Functional and behavior models for the supervision of an intelligent and autonomous system, IEEE Trans. Automation Sci. Eng. 10 (2013) 431–445.
- [19] R. El Harabi, B. Ould-Bouamama, M.K.B. Gayed, M.N. Abdelkrim, Pseudo bond graph for fault detection and isolation of an industrial chemical reactor Part I: bond graph modeling, in: Proceedings of the 2010 Spring Simulation Multiconference, Society for Computer Simulation International, 2010, p. 220.
- [20] W. Borutzky, Bond graph model-based system mode identification and mode-dependent fault thresholds for hybrid systems, Math. Comput. Model. Dyn. Syst. (2014) 1–32.
- [21] L. Chang Boon, W. Danwei, S. Arogeti, Z. Jing Bing, Causality assignment and model approximation for hybrid bond graph: fault diagnosis perspectives, IEEE Trans. Automation Sci. Eng. 7 (2010) 570–580.
- [22] S. Triki, T. Mekki, A. Kamoun, Modeling switched behavior with hybrid bond graph: application to a tank system, arXiv preprint arXiv:1402.2925, 2014.
- [23] S.A. Arogeti, W. Danwei, L. Chang Boon, L. Ming, Energy-based mode tracking of hybrid systems for FDI, IEEE Trans. Syst. Man Cybern.: Syst. 43 (2013) 14-28
- [24] Y. Ming, W. Danwei, L. Ming, H. Lei, Prognosis of hybrid systems with multiple incipient faults: augmented global analytical redundancy relations approach, IEEE Trans. Syst. Man Cybern, Part A: Syst. Hum. 41 (2011) 540–551.
- [25] G. Dauphin-Tanguy, C.S. Kam, How to model parameter uncertainties in a bond graph framework, in: Simulation in Industry, 11th European Simulation Symposium, ESS, 1999, pp. 121–125.
- [26] M.A. Djeziri, R. Merzouki, B.O. Bouamama, G. Dauphin-Tanguy, Robust fault diagnosis by using bond graph approach, IEEE/ASME Trans. Mechatronics 12 (2007) 599–611.
- [27] M.A. Djeziri, B. Ould Bouamama, R. Merzouki, Modelling and robust FDI of steam generator using uncertain bond graph model, J. Process Control 19 (2009) 149–162.
- [28] M. Jha, G. Dauphin-Tanguy, B. Ould Bouamama, Robust FDI based on LFT BG and relative activity at junction, in: 2014 European on Control Conference (ECC), IEEE, 2014, pp. 938–943.
- [29] M.S. Jha, Diagnostics and prognostics of uncertain dynamical systems in a bond graph framework Ph.D. Thesis, Ecole Centrale de Lille, 2015, pp. 51–100.
- [30] R.E. Moore, Methods and Applications of Interval Analysis, SIAM, 1979.
- [31] R.E. Moore, R.B. Kearfott, M.J. Cloud, Introduction to Interval Analysis, Siam, 2009.
- [32] W. Zhang, J. Liu, C. Cho, X. Han, A hybrid parameter identification method based on Bayesian approach and interval analysis for uncertain structures, Mech. Syst. Signal Process, 60–61 (2015) 853–865.
- [33] M.S. Jha, G. Dauphin-Tanguy, B. Ould-Bouamama, Particle filter based hybrid prognostics for health monitoring of uncertain systems in bond graph framework, Mech. Syst. Signal Process. 75 (2016) 301–329.
- [34] G.B. Dantzig, B.C. Eaves, Fourier-Motzkin elimination and its dual, J. Comb. Theory, Ser. A 14 (1973) 288-297.
- [35] A. Frank, Z. Király, B. Kotnyek, An algorithm for node-capacitated ring routing, Oper. Res. Lett. 35 (2007) 385–391.
- [36] E. Hansen, G.W. Walster, Global Optimization Using Interval Analysis: Revised and Expanded, CRC Press, 2003.
- [37] J. Armengol Llobet, Application of Modal Interval Analysis to the Simulation of the Behaviour of Dynamic Systems with Uncertain Parameters, Universitat de Girona, 2000.
- [38] L. Jaulin, E. Walter, Set inversion via interval analysis for nonlinear bounded-error estimation, Automatica 29 (1993) 1053-1064.
- [39] A.K. Samantaray, K. Medjaher, B. Ould Bouamama, M. Staroswiecki, G. Dauphin-Tanguy, Diagnostic bond graphs for online fault detection and isolation, Simul. Model. Pract. Theory 14 (2006) 237–262.
- [40] A.K. Samantaray, B.O. Bouamama, Model-based Process Supervision: A Bond Graph Approach, Springer Science & Business Media, 2008.
- [41] B.O. Bouamama, A. Samantaray, M. Staroswiecki, G. Dauphin-Tanguy, Derivation of constraint relations from bond graph models for fault detection and isolation, Simul. Ser. 35 (2003) 104–109.
- [42] H.P. Williams, Fourier-Motzkin elimination extension to integer programming problems, J. Comb. Theory, Ser. A 21 (1976) 118–123.
- [43] A. Levant, Robust exact differentiation via sliding mode technique, Automatica 34 (1998) 379–384.
- [44] A. Levant, Universal single-input-single-output (SISO) sliding-mode controllers with finite-time convergence, IEEE Trans. Automatic Control 46 (2001) 1447–1451.
- [45] E. Tarasov, C. Sueur, B.O. Bouamama, G. Dauphin-Tanguy, Flat control of a torsion bar with unknown input estimation, in: 2014 IEEE Conference on Control Applications (CCA), IEEE, 2014, pp. 2054–2059.
- [46] C. Kleijn, Torsion Bar 2.0 Reference Manual, Controllab Products B.V, Enschede, 2011.
- [47] S.M. Rump, INTLAB—Interval Laboratory, Springer, 1999.
- [48] V. Venkatasubramanian, R. Rengaswamy, K. Yin, S.N. Kavuri, A review of process fault detection and diagnosis: Part I: quantitative model-based methods, Comput. Chem. Eng. 27 (2003) 293–311.
- [49] M. Taleb, A. Levant, F. Plestan, Pneumatic actuator control, Solution based on adaptive twisting and experimentation, Control Eng. Pract. 21 (2013) 727–736.